ELSEVIER

Journal of Photochemistry and Photobiology A: Chemistry 112 (1998) 117–125

Journal of Photochemistry and Photobiology A:Chemistry

Photophysics of the naphthalene–anthracene bichromophoric molecular system in a supersonic jet expansion

Gershon Rosenblum, Shammai Speiser *

Department of Chemistry, Technion, Israel Institute of Technology, Haifa 32000, Israel

Abstract

Intramolecular electronic energy transfer (intra-EET) was investigated in an isolated bichromophoric naphthalene (**N**) and anthracene (**A**) 1:1 molecular cluster. Investigation of the spectroscopic properties of these chromophores, separately and loosely bound in a van der Waals complex, helps to understand the dependence of the EET rate on the initially excited vibronic level and on the cluster's interchromophoric orientation. Measurement of fluorescence excitation spectra of anthracene, at different anthracene pressures shows bands that can be assigned to dimers of anthracene. From measurement of the anthracene excitation spectrum at increasing naphthalene pressures one can identify other spectral features, characterized by different spectral shifts from excitations of the bare molecule. Some transitions are probably due to a 13.5 cm^{-1} progression associated with an interchromophore cluster bond. Pressure dependence of fluorescence intensity gives evidence for 1:1 cluster composition, and for a slow intra-EET rate that is associated with an unfavoured orientation of the two chromophores in one of the two possible conformers of the **A–N** cluster, as supported by a calculation of the cluster geometry and by comparison with a recent study of intra-EET in the **A–(CH$_2$)$_n$–N** bichromophoric molecules.

Keywords: Naphthalene; Anthracene; Intra-EET

1. Introduction

Electronic energy transfer (EET) process is one of the most common relaxation mechanisms of an excited chromophore. Its understanding is important for studying the natural photosynthetic processes, light harvesting, polymer photophysics, dye laser operation, light interaction with molecular crystals and photochemical synthesis [1]. EET was studied extensively in condensed systems and its mechanisms are now thought to be well understood [e.g., Refs. [1–8]].

EET may be promoted either through, Coulombic dipole–dipole interaction or through electron exchange. The first case was formulated by Förster [9,10] who showed that the EET rate constant for donor and acceptor at a distance R_{DA}, is given by

$$k_{ET}^{dd} = \frac{9000 \ln 10\, \Gamma^2\, \Phi_D}{128\pi^5 n^4 N_A \tau_D} \frac{1}{R_{DA}^6} \int \overline{F_D}(\bar{\nu}) \varepsilon_A(\bar{\nu}) \bar{\nu}^{-4} d\bar{\nu} \equiv \frac{1}{\tau_D}\left(\frac{R_0}{R_{DA}}\right)^6 \quad (1)$$

here Φ and τ are fluorescence quantum yield and lifetime, n is refractive index of the medium, F is fluorescence spectrum and ε is absorption spectrum. Thus Förster critical transfer radius R_0 defined here and the EET rate can be calculated from spectroscopic experimental data.

In cases where the Coulomb mechanism contribution is either small or spin forbidden, the interaction can be expressed via the exchange integral. At large enough separations this integral dependence on the interchromophore distance can be approximated by the exponential chromophore wavefunctions spatial overlap dependence [11] leading to the following expression for the EET rate constant:

$$k_{ET}^{ex} = \frac{2\pi}{\hbar} K J \exp(-R_{DA}/L) \quad (2)$$

here L is an average decay radius of wavefunctions of the two interacting states, K is a constant and J is the spectral overlap integral.

It can be seen from Eqs. (1) and (2) that the Förster mechanism rate is proportional to R_{DA}^{-6}, and this interaction is most important at intermediate separations. At close separations were the wavefunctions overlap becomes considerable, the exchange mechanism dominates.

Förster critical transfer radius for most systems in solution is between 10 and 100 Å. Eq. (1) is widely used to describe

* Corresponding author.

1010-6030/98/$19.00
PII S1010-6030(97)00275-X

energy transfer in condensed phase [1]. At distances less than about 5 Å the Dexter exchange mechanism usually becomes more important [1,3]. In real systems the exchange integral evaluation by computational methods is extremely complicated, and without it the model mechanism can be employed only in some very limited cases. Still, such computations were performed in a study of series of bichromophoric molecules, yielding good agreement with experimental data on distance and orientation dependence of the EET rate [12–15].

In addition, more complicated mechanisms than the two considered in Eq. 5 can contribute to the pure electronic interaction matrix element. Notably, higher electronic levels for which wavefunctions are localized spatially between the two chromophores, can mediate the transfer. This effect ('superexchange') was detected in bichromophoric molecules, where the rigid bridge connecting the chromophores enhanced the exchange mechanism rate [5,16–19].

When the donor chromophore is excited to some specific vibronic state, it can undergo dephasing via intramolecular vibrational redistribution, (IVR), involving other molecular states that have low Franck–Condon factors for excitation (dark states).

Thus the situation under supersonic jet cooling conditions is different from the well-studied situation in condensed phase experiments. The geometry of the bichromophoric unit is usually well defined. The effect of the relative orientations of the chromophores on the EET rate can thus be conveniently studied under jet conditions. The chromophores are no longer coupled to the low frequency solvent vibrational bath. Consequently, no vibrational relaxation occurs prior to the EET process. Thus the EET process from a specific vibronic level can be studied, and the density of the coupled states is better defined.

The EET rate depends on the vibronic level choice due to the changes in the density of states. The density of vibronic states of the acceptor chromophore can be so low that the equidistant quasi-continuum model may fail and specific vibronic level structure must be considered. The other source of the rate dependence on the vibronic level is the change in the geometry of the unit that is affected by the vibrations.

The definition of a bichromophoric molecule is less straightforward in a jet experiment. It is usual to define molecule as a bichromophoric one if it can be excited to different electronic levels with excitation being localized at different parts of the molecule (chromophores). Practically, in solution experiments, the interchromophore interaction matrix element has to be less than the experimental spectral resolution. This resolution is limited by the solvent and the temperature effects. All organic molecules for which the two chromophores are not conjugated, can be safely considered bichromophoric. The vibronic relaxation in solution is usually faster than the interchromophore interaction rate in the non-conjugated molecules, and this can also serve as a criterion for whether or not the molecule is bichromophoric.

Intramolecular EET (intra-EET) in a bichromophoric cluster, was detected for the first time under the supersonic jet cooling conditions by Poetl and McVey in benzoic acid dimers [20]. Tomioka et al. [21] reported EET in the very similar system of heterocluster of benzoic and *p*-toluic acids. A better resolution in the fluorescence excitation and emission spectra was achieved in this work, providing more information on the EET process. Lahmani et al. [22] studied EET in *p*-xylene–*p*-difluorobenzene clusters. The study of *s*-tetrazine dimers by Haynam et al. and Young et al. revealed the manifestation of two isomers in the intra-EET dynamics [23,24].

Previous research in our laboratory of EET in molecular clusters [25–28] was performed with benzene–biacetyl and naphthalene–anthracene clusters (**N–A**). These clusters are very much different from the ones studied in the works described above. The energy gap between the donor and the acceptor electronic origin transitions is rather large (15 909 cm^{-1} and 4505 cm^{-1} respectively). The density of the intramolecular vibrational states of the acceptor at the energy corresponding to the donor excitation is extreme. The cluster stationary state at this energy is localized on the acceptor to a very high degree. The almost solution-like coupling to the quasi-continuum of the low-frequency interchromophore modes must be added to complete the picture. The EET behaviour of different donor vibronic excited states is unlikely to be affected by an 'accidental energy overlap' with an acceptor state with a high Franck–Condon factor. Effects such as 'EET threshold excess energy' phenomenon, resulting from such discrimination of some donor vibronic levels by the non-monotonous state density of the acceptor are not very likely. The differences between the EET rates from different vibronic states, apart from a slow monotonous effect of the state density, should originate from the mean geometry changes due to vibrational motion, from possible chromophore and cluster symmetry breaking and from vibration-specific coupling between the vibrational modes of the two chromophores via the interchromophore modes. The preliminary work in **N–A** clusters [26] was extended and is described in the present paper.

2. The naphthalene–anthracene bichromophoric molecular system

Anthracene first singlet electronic transition origin is at 27 695 cm^{-1} [29]. The pure electronic transition is polarized along the short axis, and the transition dipole moment in solution is 9.2×10^{-30} C m [18] (this value can be obtained also from the integrated anthracene absorption spectrum [30]). The fluorescence quantum yield is 0.36 [30]. The second electronic transition origin is at about 30 500 cm^{-1}, polarized along the long axis. The oscillator strength of this transition is an order of magnitude lower than that of the first one. Consequently, at any excitation energy above 30 500 cm^{-1} the vibrational mixing between the two electronic states

ensures that anthracene stationary states exhibit spectroscopic properties typical of the first transition [18]. The contribution of the second transition to the overall density of states at higher energies can be safely neglected.

The first singlet electronic transition (32 020 cm^{-1}) of naphthalene is polarized along the long axis, but it has a very low oscillator strength (~0.0002 [18], ~0.001 [31], ~0.002 [32], ~0.003 [33], depending on the solvent and on the degree of involvement of the higher transitions in the integration of the corresponding spectral band). The pure S_1 electronic transition dipole moment is 4×10^{-31} C m [18,30]. The fluorescence quantum yield is 0.23 [30]. The vibronic bands gain intensity from coupling to the higher singlet electronic states, mainly to S_2 at 35 806 cm^{-1} and to S_3, depending on the vibrational symmetry [31,34,35]. The intense vibronic transitions in naphthalene are thus short axis polarized. The transition dipole moment of the most intense vibronic transition, $8(b_{1g})_0^1$ at $\Delta\upsilon_n=438$ cm^{-1}, is about 1×10^{-30} C m.

The fluorescence decay lifetime of the anthracene excited at its origin transition in solution is 5 ns [32,36]. In the cold free molecules in the jet this value is ~24 ns [37,38]. At excess vibronic energies of 4500–5000 cm^{-1}, relevant to the present work, lifetimes of the vibronic transitions in the jet are 4–5 ns. The naphthalene lifetime in solution is 100–120 ns depending on the solvent [36]. Lifetimes of the naphthalene origin transition and of the lowest vibronic transitions are between 270–320 ns in jet experiments [39]. The anthracene origin transition fluorescence quantum yield in the jet is 0.67 [40]. The fluorescence quantum yield of the naphthalene $8(b_{1g})_0^1$ transition is 0.35 [34]. Fig. 1 depicts schematically the energy levels and relevant photophysical parameters for the **N–A** system.

The Förster radius for EET from naphthalene to anthracene in solution, calculated from the spectral data is 23.2 Å [41]. This implies an EET rate of 2.5×10^{11} s^{-1} at a typical sandwich cluster separation of 3.57 Å. This estimate is, of course, very crude. It does not take into account the exchange mechanism. In addition, at such short distances the dipole–dipole picture is not accurate, and contributions from higher Coulomb terms must be included [3].

Naphthalene excitation spectrum under jet cooled conditions was recorded by Beck et al. over a wide spectral range, and many transitions were assigned [42]. Anthracene excitation spectrum and some vibronic assignments can be found in a work by Lambert et al. [29].

The *first* spectroscopic study of bichromophoric molecules containing naphthalene and anthracene chromophore in solution was performed by Schnepp and Levy [43]. In fact, it was the first EET study in a bichromophoric molecule. The three studied molecules contained 9-anthryl and 1-naphthyl linked by a one (**A1N**), two (**A2N**) and three methylene (**A3N**) flexible chain. It was found for all the molecules that all the fluorescence signal following the naphthalene moiety excitation originated from the anthracene moiety. This corresponded to a complete intra-EET process. Several more studies of these molecules followed [e.g., Refs. [44–51]]. EET was studied also in a bichromophoric molecule containing the two chromophores linked by a rigid bridge consisting of norbornyl and bicyclohexane units [18]. Evidence was found of the bridge mediated superexchange intra-EET mechanism in this molecule.

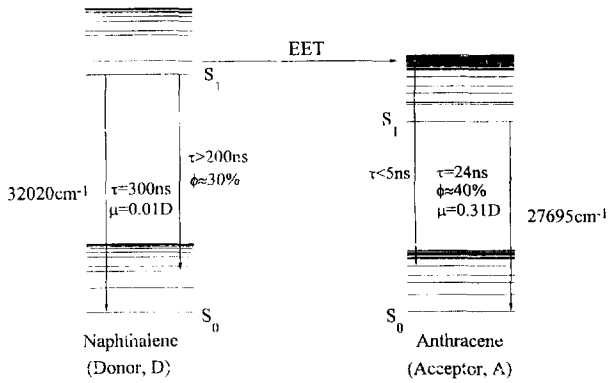

Fig. 1. Photophysical parameters (lifetime τ, fluorescence quantum yield ϕ and transition dipole moment μ) of the bichromophoric system naphthalene–anthracene. The shown values are for bare naphthalene and anthracene molecules under the supersonic jet conditions. Corresponding values for the chromophores in clusters and in bichromophoric molecules can be slightly different.

3. Experimental

Naphthalene–anthracene gas mixtures were prepared by passing He at 4–5 atm. over, naphthalene held at 50°C in the gas entrance of a high-temperature solenoid valve. The valve, built according to the design of Lubman and Kronick [52], Tembreull et al. [53] and Li and Lubman [54], serves as the hot oven and contains the added anthracene. The hot oven in the valve is separated from the solenoid by a water jacket which serves to control the naphthalene temperature and to protect the solenoid and the spring.

The gas mixture was expanded through a 1 mm orifice into a stainless steel vacuum chamber. The chamber was pumped by an untrapped CVC Goldine 6″ diffusion pump backed by a Welch model 1397 rotary pump. Typical background pressure was about 10^{-4} Torr.

The samples were excited by a Quanta-Ray PDL-1 Dye laser, pumped by the second harmonic of a DCR Nd:YAG laser, operated at 10 Hz, or by a Continuum integrated laser system. Frequency doubled rodamine 640 was used to excite naphthalene, while anthracene excitation was provided by frequency doubling the output of the dye laser operating with LDS-698, using WEX-1 wavelength extender. The laser light was passed through a series of baffles into a vacuum chamber, and intersected the molecular beam about 35 mm from the valve orifice, where *the number of molecular collisions is very small.*

Excitation spectra were recorded with a Hamamatsu R777 photomultiplier tube using appropriate filters to exclude

undesired light. A spex 0.22 m monochromator was used to record dispersed emission spectra. Signals were averaged over a number of laser shots with Textronix 2400 digital oscilloscope. The overall time resolution of the system was 10 ns.

4. Results and discussion

The electronic origin of the first singlet transition ($S_1 \leftarrow S_0$, 0_0^0) band of anthracene was found at approximately 27 696 cm^{-1}. The accepted literature value is 27 695 cm^{-1} [e.g., Ref. [55]], and we attribute the apparent ~1 cm^{-1} mismatch to the dye laser calibration differences, and to rotational temperature effects. All shifts from the anthracene 0_0^0 transition frequency that are mentioned below ($\Delta\upsilon_a$) were calculated with respect to the 27 695.0 cm^{-1} value, for convenience purposes, since our measured 0_0^0 band actual center position varied between ~27 695.5 cm^{-1} and ~27 697 cm^{-1} depending on the experiment conditions.

The spectral width of our excitation laser beam (~0.2 cm^{-1}) was far larger than the estimated spacing between the individual anthracene rovibronic lines (~0.03 cm^{-1}) [39,56]. The observed bands in fact represented rotational envelopes formed due to the lack of rotational spectral resolution. The vibronic line shape was thus affected by the symmetry of the transition. Moreover, it was possible to deduce information on the rotational temperature distribution from the apparent width of the vibronic lines [29,55]. The 0_0^0 band spectral width at half maximum was usually between 1.2 cm^{-1} and 2.2 cm^{-1}, depending on the expansion cooling conditions. This corresponded to average rotational temperatures between ~1 K and ~3 K [29,55] which are significantly lower than in previous works [29,55]. In a control experiment with a low (2 atm.) helium stagnation pressure and with an artificially inhibited pumping, a 2.9 cm^{-1} band width was obtained, which was closer to the literature results (3.3 cm^{-1}, [29]), and corresponded to the rotational temperature of ~5 K.

The excitation spectrum of anthracene at a region red shifted with respect to the 0_0^0 transition, is shown in Fig. 2. Lambert et al. reported that the bands at $\Delta\upsilon_a$ values of 54 cm^{-1} and at 157 cm^{-1} were anthracene hot bands [29]. They observed also the bands at 21 cm^{-1} and at 41 cm^{-1}. Their 61 cm^{-1} shifted band evidently corresponds to our 59.5 cm^{-1} and 62.5 cm^{-1} bands. This is consistent with our better apparent cooling that resulted in smaller rotational band widths and in better resolution.

There is no decisive proof that all the bands observed to the red of the anthracene 0_0^0 transitions are hot bands. The 21 cm^{-1} band might correspond to an excitation of helium–anthracene cluster. It is possible that some bands originate from an anthracene dimer, although it was improbable since the dimer activity was not expected in the studied spectral region. The possibility of a signal from some impurities in anthracene can be ruled out since the detected spectra did not depend on the anthracene sample origin or its preparation.

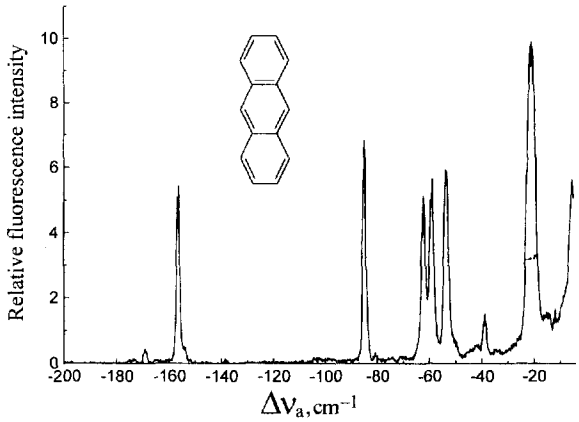

Fig. 2. Anthracene excitation spectrum at a region red shifted from the 0_0^0 transition.

The anthracene spectral activity farther to the red from the 0_0^0 transition is rather limited (Fig. 3). The 392 cm^{-1} band corresponded to the $(12a_g)_1^0$ transition. Only one other band was detected in this region. This was convenient for the following cluster study, since the cluster bands were expected in this spectral region.

Introducing naphthalene into the jet resulted in appearance of a complex spectral structure (Fig. 4). Many new bands

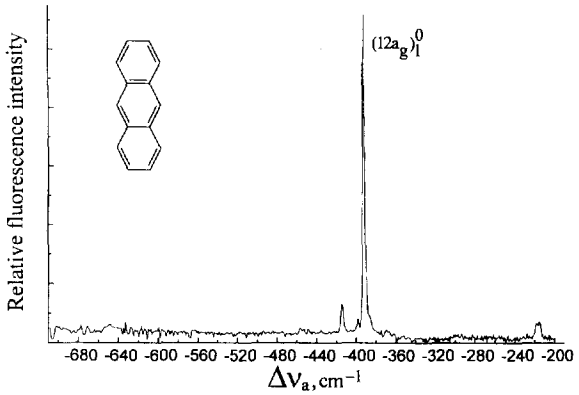

Fig. 3. Anthracene excitation spectrum, showing $(12a_g)_0^1$ band.

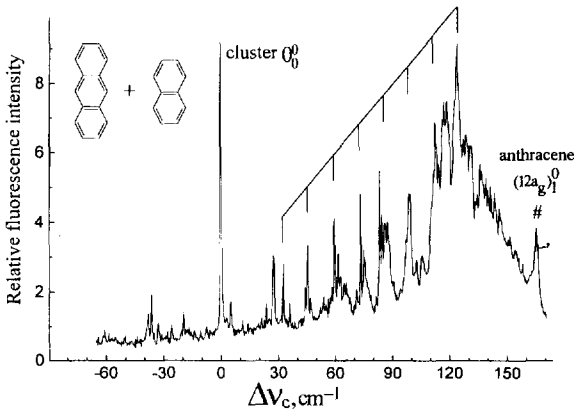

Fig. 4. Anthracene spectrum upon addition of naphthalene. The band marked with # originates from bare anthracene. Other bands originate from anthracene moiety in naphthalene–anthracene cluster.

Table 1
Cluster spectrum in anthracene moiety origin transition spectral region

$\Delta\upsilon_a$, cm^{-1}	$\Delta\upsilon_c$, cm^{-1}	Typical relative intensity	Assignment (step, cm^{-1})
591.8	−36.1	1.9	
575.3	−19.6	1.4	
555.7	0	9.2	0_0^0
550.5	5.2	1.7	
527.8	27.9	3.0	
523.0	32.7	2.8	A_0^1 (22.7)
509.8	45.9	3.4	$A_0^1 X_0^1$ (13.2)
495.9	59.8	4.1	$A_0^1 X_0^2$ (13.9)
482.5	73.2	4.8	$A_0^1 X_0^3$ (13.4)
480.7	75.0	3.2	
469.6	86.1	5.5	$A_0^1 X_0^4$ (12.9)
456.3	99.4	4.8	$A_0^1 X_0^5$ (13.3)
442.9	112.8	6.9	$A_0^1 X_0^6$ (13.4)
437.6	118.1	7.3	
431.0	124.7	9.2	$A_0^1 X_0^8$ (11.9)
418.8	136.9	5.7	$A_0^1 X_0^9$ (12.2)
192.6	363.1	0.3	
165.7	390.0	1.9	$(12a_g)_0^1$
152.8	402.9	0.5	
148.2	407.5	0.2	
140.3	415.4	0.2	
103.6	452.1	1.1	isomer?

were resolved (Table 1). The linear dependence of the bands intensity on the vapour pressures of the two substances (Figs. 5 and 6) prove that these spectral features originated from the naphthalene–anthracene 1:1 cluster.

The strongest band at the red end of the spectrum (at 556 cm^{-1}) was tentatively assigned as the 0_0^0 transition of the anthracene moiety in the cluster. Shifts of cluster bands with respect to this band ($\Delta\upsilon_c$) are shown. An approximately equidistant (~ 13.4 cm^{-1}) progression of at least nine bands was identified. It was assigned to a 'slide' interchromophore vibration of a sandwich cluster. The spectrum is very similar to the anthracene–benzene cluster spectrum [56], indicating an involvement of similar cluster vibrational modes.

In an earlier study in our laboratory [26,28], naphthalene–anthracene cluster spectrum was measured at a higher energy spectral region. An equidistant progression (interval of ~ 13.8 cm^{-1}) was found at about 500 cm^{-1} above the bare anthracene origin. In Table 2 frequencies of these transitions are compared to the corresponding ones found in the present work. It is evident from this comparison, that the previously found progression corresponds to an excitation of the same interchromophore vibration combined with an intrachromophore vibration of anthracene of 1020 cm^{-1}. This is the well studied $(9a_g)_0^1$ transition of anthracene [29]. If this assignment was correct, the cluster band corresponding to the $(9a_g)_0^1$ transition could not be observed due to its overlap with the bare anthracene $(10b_{1g})_0^1$ band. The $9a_g + A + 4X$ band was not observed since it overlapped with the bare anthracene $(11b_{1g})_0^2$ band.

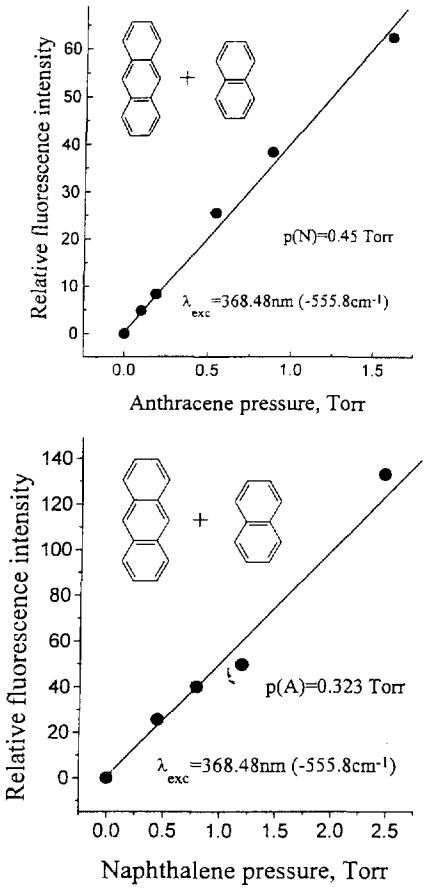

Fig. 5. Cluster origin band signal versus vapour pressure of the parent substances.

A marked intensity loss with increasing cluster excess vibrational energy was observed at ~ 150 cm^{-1} above the cluster electronic transition. At such excess energies the interchromophore vibrational state density is already high and the six cluster modes are completely mixed. The vibrational levels at these energies correspond to a large amplitude chaotic motions in the cluster, and hence the marked decrease in the Franck–Condon factors.

No cluster bands were detected at higher excess energies, apart from some activity at about 400 cm^{-1} above the cluster 0_0^0 transition frequency (Fig. 7). The strongest band at 390.0 cm^{-1} above the origin is most likely the $(12a_g)_0^1$ transition in the anthracene moiety. Other cluster transitions in this region possibly include interchromophore vibrational excitation combined with the anthracene $12a_g$ vibration excitation. The presence of the spectral structure around the anthracene chromophore vibronic transition frequency manifests the weak coupling between the intra-aromatic vibrational mode and the isoenergetic quasi-continuum of the interchromophore modes.

The band at 104 cm^{-1} does not correspond to any anthracene moiety intramolecular vibration. Most likely it originated from an isomer of the cluster with weaker anthracene electronic system perturbation by naphthalene. This would

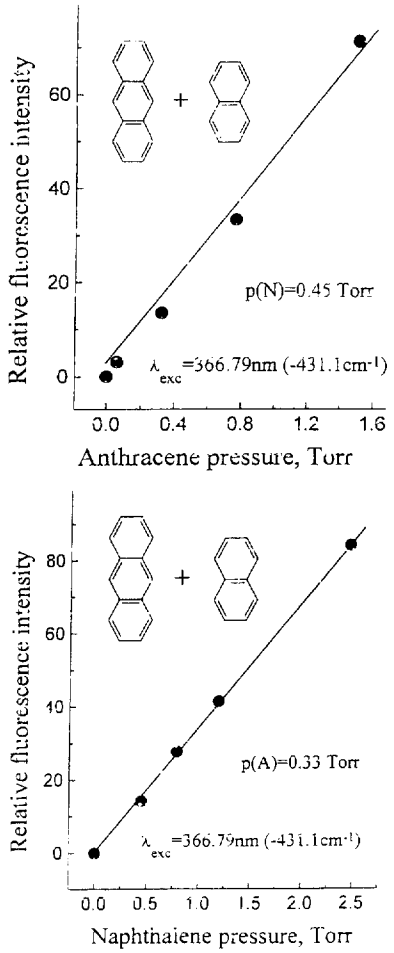

Fig. 6. Cluster 125 cm^{-1} band signal versus vapour pressure of the parent substances.

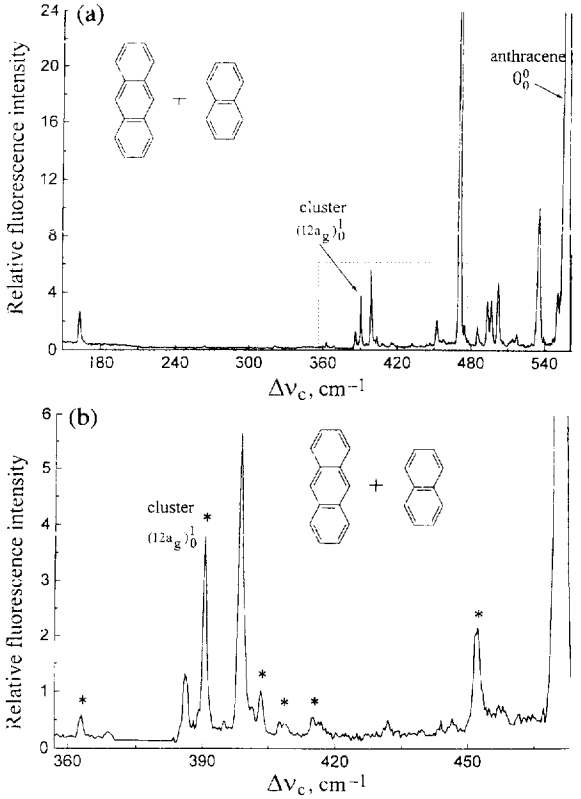

Fig. 7. (a) Anthracene spectrum upon addition of naphthalene. (b) Same as a, the region of the cluster activity being enlarged. The bands marked with * originate from anthracene moiety in naphthalene–anthracene cluster.

be consistent with the spectrum of the naphthalene moiety (see below).

No new features appeared in naphthalene spectrum upon introduction of anthracene [26,28]. The bare anthracene fluorescence excitation continuum in this region forced us to exclude the first 25 ns of the signal and to monitor only the naphthalene-like long lifetime fluorescence. Any possible signal originating from excitation of the anthracene moiety in the cluster was anyway hindered by this continuum.

Bare naphthalene bands intensity appeared to decrease with addition of anthracene. It led previously to an incorrect conclusion that these bands were quenched by the cluster formation [26,28]. It was found that the present anthracene amount was not enough to quench the naphthalene fluorescence intensity by the detected ratios even if all of the anthracene would have formed clusters with naphthalene. The main reason for the naphthalene spectrum intensity decrease was found to be the initial temperature increase necessary for the introduction of anthracene. The initial temperature increase was found to reduce the intensities of the naphthalene transitions even without anthracene sample in the lower cell. The initial temperature increase resulted in the rise of the final jet

Table 2
Assignment of previously found [26,28] cluster bands

This work (I)		Assignment (step, cm^{-1})	Previous work [26,28] (II)		(II)–(I), cm^{-1}	Assignment (step, cm^{-1})
$\Delta\upsilon_a$, cm^{-1}	$\Delta\upsilon_c$, cm^{-1}		$\Delta\upsilon_a$, cm^{-1}	$\Delta\upsilon_c$, cm^{-1}		
−555.7	0	0_0^0	–	–	–	masked by $(10b_{1g})_0^1$
−523.0	32.7	A_0^1 (22.7)	496.6	1052.3	1019.6	$(9a_g)_0^1 A_0^1$
−509.8	45.9	$A_0^1 X_0^1$ (13.2)	510.3	1066.0	1020.1	$(9a_g)_0^1 A_0^1 X_0^1$ (13.7)
−495.9	59.8	$A_0^1 X_0^2$ (13.9)	523.9	1079.6	1019.8	$(9a_g)_0^1 A_0^1 X_0^2$ (13.6)
−482.5	73.2	$A_0^1 X_0^3$ (13.4)	538.0	1093.7	1020.5	$(9a_g)_0^1 A_0^1 X_0^3$ (14.1)
−469.6	86.1	$A_0^1 X_0^4$ (12.9)	–	–	–	masked by $(11b_{1g})_0^2$
−456.3	99.4	$A_0^1 X_0^5$ (13.3)	566.6	1122.3	1022.9	$(9a_g)_0^1 A_0^1 X_0^5$ (?)

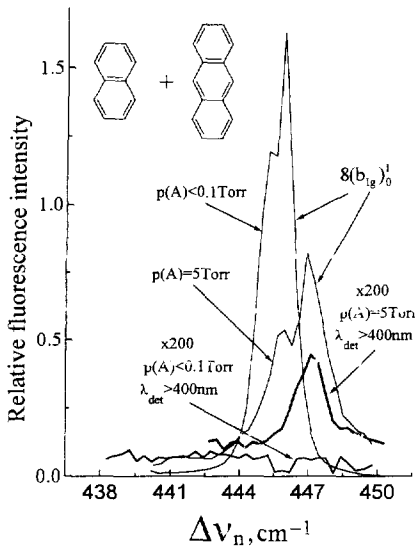

Fig. 8. Cluster band observed with a 399 nm cut-off filter that absorbed completely the bare naphthalene $8(b_{1g})_0^1$ band signal. Naphthalene vapour pressure 0.45 Torr for all cases.

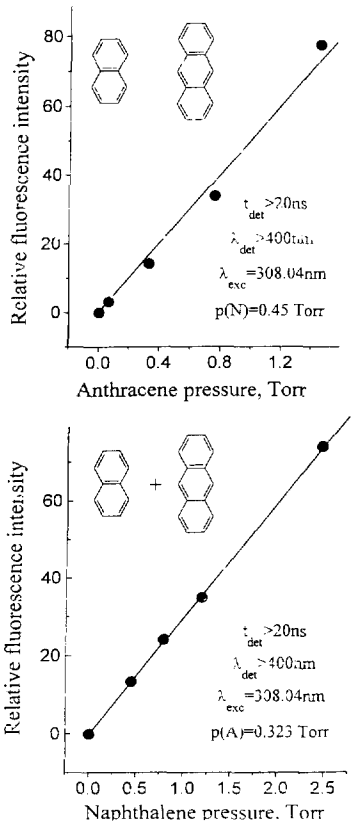

Fig. 9. Cluster band signal versus vapour pressure of the parent substances.

temperature and consequent broadening and lowering of the detected rotational envelopes of the vibronic bands. However, it is not possible to exclude quenching as a minor contributor to the observed effect.

The only detected spectral feature that depends on the presence of anthracene was found to overlap with the strongest band of bare naphthalene, $8(b_{1g})_0^1$. It was found that the

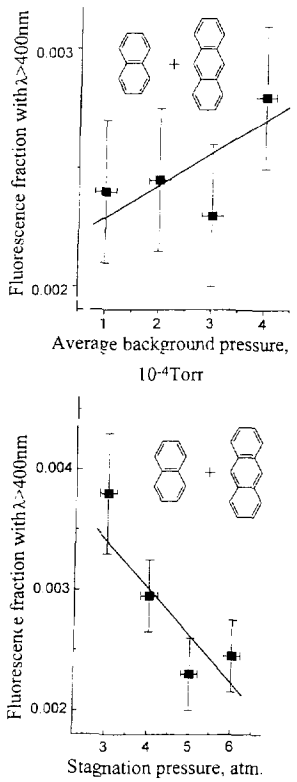

Fig. 10. Cluster band intensity at different cooling conditions.

introduction of the 399 nm cut-off filter normally known [28] to completely absorb bare naphthalene fluorescence, failed to do so in presence of anthracene (Fig. 8). The intensity of this weak band, detected in presence of the filter, depends linearly (Fig. 9) on both anthracene and naphthalene vapour pressure. This indicates that the band originates from a 1:1 naphthalene–anthracene cluster. The signal was long-lived, with a decay lifetime of 100 ns $< \tau <$ 200 ns, which is somewhat less than the lifetime of bare naphthalene. More accurate lifetime estimations were impossible due to the low signal intensity.

The intensity ratio of the cluster band to the unfiltered bare naphthalene band was found to depend on cooling conditions. The cluster band was generally weaker when the cooling was more efficient (Fig. 10). Such behaviour is typical for hot bands. However, the detected band could hardly be a hot band, since some stronger bands should have been observed in this case. More probably, the band originates from a minor cluster isomer, corresponding to a local minimum on the interchromophore potential surface. Relative population of such a minimum is smaller under efficient cooling conditions, since it competes with population of the global minimum. The existence of such an isomer is supported by our calculation of cluster geometries [56].

We can summarize that two major observations were made upon excitation of the naphthalene chromophore in the naphthalene–anthracene cluster. The first observation is the *absence* of the cluster bands in the *unfiltered* spectrum. Cluster formation has been proven by the spectra of the anthracene moiety that were recorded under the same experimental con-

ditions. There is no reason to believe that the naphthalene moiety in the cluster should not absorb the light at specific characteristic frequencies. Nevertheless, its fluorescence following such an excitation was not detected. The most probable explanation is that intra-EET from naphthalene is much faster than the fluorescence decay, and that the naphthalene moiety fluorescence was thus kinetically suppressed [26,28]. The fast anthracene moiety fluorescence which necessarily resulted from such process had escaped detection due to masking by the bare anthracene fluorescence. Another possible explanation for fluorescence quenching is a fast cluster dissociation, since the excess energy acquired by the anthracene moiety is almost twice as large as the cluster binding energy. Such dissociation could enhance the non-radiative processes in the anthracene moiety, such as triplet formation or internal conversion to the ground electronic level. Alternatively, the energy could have been lost by anthracene molecule fluorescence following the dissociation. In this case the fluorescence would escape detection for the same reason as mentioned above. Independently from the possible evolution of the cluster following the EET, the lack of detected naphthalene moiety fluorescence indicates an intra-EET process with a rate constant of at least $1\times10^{8}\ s^{-1}$.

Our second observation was the detection of a weak cluster band in the filtered spectrum, consisting of anthracene emission. Its shift from the parent bare naphthalene band was minimal ($\sim1\ cm^{-1}$), and its intensity was far lower (between 10 and 100 times) than what could have been expected from comparison of the anthracene moiety signal with the bare anthracene signal. The estimated long lifetime of the band (~150 ns), when compared to the parent naphthalene band lifetime of 270 ns, indicates a slow EET process (a rate constant of between $1\times10^{6}\ s^{-1}$ and $3\times10^{6}\ s^{-1}$). It can be concluded from the lower than expected intensity, that the band originated from a minor 1:1 cluster isomer in the jet. The perturbation of the naphthalene chromophore electronic structure by anthracene should have been extremely small in this isomer to explain the observed modest spectral shift. This would mean that the chromophores were far apart in the cluster, in accord with the detected slow EET process. These observations are consistent with calculations of cluster geometries [56] and with recent EET studies on **A–N** bichromophoric molecules [57]. The possibility that the weak cluster band close to the $8b_{1g}$ bond of naphthalene is due to intramolecular exciplex formation can be ruled out since an exciplex is likely to be formed much faster than the time window of <100 ns used for the experiment.

5. Summary

We have found evidence for both efficient and inefficient EET process, that occurred in different isomers of the naphthalene–anthracene 1:1 bichromophoric molecular cluster. The efficient EET was associated with the dominant isomer and with stronger interchromophore interaction that was manifested in larger spectral shifts. The slow EET process corresponded to a minor isomer or isomers, and corresponded to smaller spectral shifts.

Cluster geometry calculations have supported this picture [56]. The linear minor isomer was predicted along with the common sandwich-type isomer. In addition, recently bichromophoric molecules containing the anthracene and naphthalene moieties linked by one methylene (**A1N**), three methylene (**A3N**) and six methylene (**A6N**) chains were studied [57]. The anthracene moiety spectra of **A3N** and **A6N** appeared to be almost identical, consisting of many congested bands, and differing only in features attributable to minor conformers. The two spectra were qualitatively similar in many ways to the naphthalene–anthracene cluster spectrum. This agreed well with the expected sandwich-type conformations of both molecules. The EET process in **A3N** was found to be almost complete ($k_{EET}>1\times10^{9}\ s^{-1}$), with residual naphthalene-like fluorescence probably arising from molecules that were not sufficiently cooled. In **A6N** the EET process accounted for all the observed fluorescence.

The behaviour of **A1N** molecule was quite different. The anthracene moiety spectra implied a much more rigid structure with a weaker interchromophore interaction, compared to the other two molecules. A rich naphthalene moiety spectrum was observed for two distinct **A1N** conformers, indicating a EET process at least 1000 times slower ($k_{EET}<5\times10^{5}\ s^{-1}$) than in **A3N** and **A6N**. The EET rate was measurable only for one vibronic band ($k_{EET}=4.8\times10^{6}\ s^{-1}$). In a third **A1N** conformer a faster EET process ($k_{EET}\approx1\times10^{8}\ s^{-1}$) resulted in a spectrum originating almost from the anthracene chromophore.

Molecular geometry differences are thought to be responsible for the different EET efficiencies in the bichromophoric molecules and in the **A1N** conformers, as it is in the two cluster isomers. The different behaviour of **A1N** in the jet from that in solution is the first observation of such kind.

Acknowledgements

This study was partially supported by grants from the VPR Technion Research Fund and by the Fund for the Promotion of Research at the Technion. We are grateful to the referee of this paper for constructive suggestions.

References

[1] S. Speiser, Chem. Rev. 96 (1996) 1953.
[2] S.H. Lin, W.Z. Xiao, W. Dietz, Phys. Rev. E 47 (1993) 3698.
[3] G.D. Scholes, K.P. Ghiggino, J. Photochem. Photobiol. A: Chem. 80 (1994) 355.
[4] R.D. Harcourt, K.P. Ghiggino, G.D. Scholes, S. Speiser, J. Chem. Phys. 105 (1996) 1897.
[5] G.D. Scholes, Electronic interactions and interchromophore energy transfer, PhD Thesis, University of Melbourne (1994).
[6] D.W. Liao, W.D. Cheng, J. Bigman, Y. Karni, S. Speiser, S.H. Lin, J. Chin. Chem. Soc. 42 (1995) 177.

[7] S. Speiser, J. Photochem. 22 (1983) 195.
[8] S. Speiser, J. Katriel, Chem. Phys. Lett. 102 (1983) 88.
[9] Th. Förster, Discuss. Faraday. Soc. 27 (1959) 7.
[10] Th. Förster, in: O. Sinanoglu (Ed.), Modern Quantum Chemistry, Vol. 3, Academic Press, New York, 93 (1968).
[11] D.L. Dexter, J. Chem. Phys. 21 (1953) 836.
[12] S.T. Levy, M.B. Rubin, S. Speiser, J. Am. Chem. Soc. 114 (1992) 10747.
[13] S.T. Levy, M.B. Rubin, S. Speiser, J. Photochem. Photobiol. A: Chem. 66 (1992) 159.
[14] S.T. Levy, S. Speiser, J. Chem. Phys. 96 (1992) 3585.
[15] S.T. Levy, Electronic energy transfer in bichromophoric molecules, MSc Thesis, Technion, Israel Institute of Technology (1992).
[16] S.A. Jonker, J.W. Verhoeven, H. Oevering, J. Kroon, M.N. Paddon-Row, A.M. Oliver, Chem. Phys. 170 (1993) 359.
[17] M. Roest, J.M. Lawson, M.N. Paddon-Row, J.W. Verhoeven, Chem. Phys. Lett. 230 (1993) 536.
[18] G.D. Scholes, K.P. Ghiggino, A.M. Oliver, M.N. Paddon-Row, J. Phys. Chem. 97 (1993) 11871.
[19] G.D. Scholes, R.D. Harcourt, K.P. Ghiggino, J. Chem. Phys. 102 (1995) 9574.
[20] D.E. Poetl, J.K. McVey, J. Chem. Phys. 80 (1984) 1801.
[21] Y. Tomioka, H. Abe, N. Mikami, M. Ito, J. Phys. Chem. 88 (1984) 5186.
[22] F. Lahmani, C. Lardeux-Dedonder, A. Zehnacker-Rentien, J. Chem. Phys. 92 (1990) 4159.
[23] C.A. Haynam, D.V. Brumbaugh, D.H. Levy, J. Chem. Phys. 79 (1983) 1592.
[24] L. Young, C.A. Haynam, D.H. Levy, J. Chem. Phys. 79 (1983) 1592.
[25] J. Bigman, Y. Karni, S. Speiser, J. Photochem. Photobiol. A: Chem. 78 (1994) 101.
[26] J. Bigman, Y. Karni, S. Speiser, Chem. Phys. 177 (1993) 601.
[27] J. Bigman, Intermolecular and intramolecular electronic energy transfer under supersonic jet cooled conditions, DSc Thesis, Technion, Israel Institute of Technology (1992).
[28] Y. Karni, Electronic energy transfer in molecular clusters, MSc Thesis, Technion, Israel Institute of Technology (1992).
[29] W.R. Lambert, P.M. Felker, J.A. Syage, A.H. Zewail, J. Chem. Phys. 81 (1984) 2195.
[30] I.B. Berlman, Handbook of Fluorescence Spectra of Aromatic Compounds, Academic Press, New York (1965).
[31] F.M. Behlen, D.B. McDonald, V. Sethuraman, S.A. Rice, J. Chem. Phys. 75 (1981) 5685.
[32] N.J. Turro, Molecular Photochemistry, W.A. Benjamin, London (1965).
[33] T. Troxler, S. Leutwyler, J. Chem. Phys. 95 (1991) 4010.
[34] M. Stockburger, H. Gattermann, W. Klusmann, J. Chem. Phys. 63 (1975) 4529.
[35] F. Lahmani, E. Breheret, A. Zehnacker-Rentien, T. Ebata, J. Chem. Soc., Faraday Trans. 89 (1993) 623.
[36] J.B. Birks, Photophysics of aromatic molecules, Wiley-Interscience, London (1970).
[37] W.R. Lambert, P.M. Felker, A.H. Zewail, J. Chem. Phys. 81 (1984) 2209.
[38] T.R. Hays, W. Henke, H.L. Selzle, E.W. Schlag, Chem. Phys. Lett. 77 (1981) 19.
[39] P.B. Bisht, H. Petek, K. Yoshihara, Chem. Phys. Lett. 213 (1993) 75.
[40] A. Amirav, J. Jortner, Chem. Phys. Lett. 132 (1986) 335.
[41] I.B. Berlman, Energy Transfer Parameters of Aromatic Compounds, Academic Press, New York (1973).
[42] S.M. Beck, D.E. Powers, J.B. Hopkins, R.E. Smalley, J. Chem. Phys. 73 (1980) 2019.
[43] O. Schnepp, M. Levy, J. Am. Chem. Soc. 84 (1962) 172.
[44] E.A. Chandross, C.J. Dempster, J. Am. Chem. Soc. 92 (1970) 3586.
[45] E.A. Chandross, H.T. Thomas, Chem. Phys. Lett. 9 (1971) 343.
[46] E.A. Chandross, A.H. Schiebel, J. Am. Chem. Soc. 95 (1973) 611.
[47] E.A. Chandross, A.H. Schiebel, J. Am. Chem. Soc. 95 (1973) 1671.
[48] J. Fergusson, A.W.H. Mau, M. Puza, Mol. Phys. 28 (1974) 1457.
[49] J. Fergusson, A.W.H. Mau, M. Puza, Mol. Phys. 28 (1974) 1467.
[50] E. Farkas, M. Hilbert, I. Ketskemety, L. Gati, Spectrochim. Acta 48A (1992) 95.
[51] Y. Mori, K. Maeda, J. Chem. Soc., Perkin Trans. 2 (1996) 113.
[52] D.M. Lubman, M.N. Kronick, Anal. Chem. 54 (1982) 660.
[53] R. Tembreull, C.H. Sin, H.M. Pang, D.M. Lubman, Anal. Chem. 57 (1985) 2911.
[54] L. Li, D.M. Lubman, Rev. Sci. Instrum. 60 (1989) 499.
[55] A. Amirav, C. Horwitz, J. Jortner, J. Chem. Phys. 88 (1988) 3092.
[56] G. Rosenblum, S. Speiser, J. Chem. Phys. 102 (1995) 9149.
[57] G. Rosenblum, D. Grosswasser, F. Schael, M.B. Rubin, S. Speiser, Chem. Phys. Lett. 263 (1996) 441.